
Faculty of Science

Faculty Publications

Variability in Biomass Burning Emissions Weakens Aerosol Forcing Due To Nonlinear Aerosol-Cloud Interactions

Kyle B. Heyblom, Hansi A. Singh, Philip J. Rasch, Haruki Hirasawa

June 2023

© 2023 Heyblom et al. This is an open access article distributed under the terms of the Creative Commons Attribution License. <https://creativecommons.org/licenses/by-nc/4.0/>

This article was originally published at:

<https://doi.org/10.1029/2022GL102685>

Citation for this paper:

Heyblom, K. B., Singh, H. A., Rasch, P. J., & Hirasawa, H. (2023). Variability in biomass burning emissions weakens aerosol forcing due to nonlinear aerosol-cloud interactions. *Geophysical Research Letters*, 50, e2022GL102685.

<https://doi.org/10.1029/2022GL102685>

Geophysical Research Letters[®]



RESEARCH LETTER

10.1029/2022GL102685

Variability in Biomass Burning Emissions Weakens Aerosol Forcing Due To Nonlinear Aerosol-Cloud Interactions

Kyle B. Heyblom¹ , Hansi A. Singh¹ , Philip J. Rasch² , and Haruki Hirasawa¹ 

¹School of Earth and Ocean Sciences, University of Victoria, Victoria, BC, Canada, ²Department of Atmospheric Science, University of Washington, Seattle, WA, USA

Key Points:

- The radiative forcing due to aerosols is overestimated if emissions are temporally-smoothed
- Interannual variability in aerosol emissions leads to a weakened time-average cloud radiative effect
- Changes in time-average cloud radiative effect with differing aerosol variability are due to nonlinear aerosol-cloud interactions

Supporting Information:

Supporting Information may be found in the online version of this article.

Correspondence to:

K. B. Heyblom,
kheyblom@uvic.ca

Citation:

Heyblom, K. B., Singh, H. A., Rasch, P. J., & Hirasawa, H. (2023). Variability in biomass burning emissions weakens aerosol forcing due to nonlinear aerosol-cloud interactions. *Geophysical Research Letters*, 50, e2022GL102685. <https://doi.org/10.1029/2022GL102685>

Received 4 JAN 2023

Accepted 27 MAR 2023

Abstract The magnitude of the aerosol forcing remains among the largest unknowns when assessing climate sensitivity over the historical period. Here, we quantify and explain a crucial but often overlooked source of uncertainty in aerosol forcing: the temporal variability of aerosol emissions. We show that time-variability in biomass burning (BB) emissions weakens the time-averaged total aerosol forcing, particularly in the Northern Hemisphere mid- to high-latitudes. BB emissions variability produces weaker (less negative) mean effective radiative forcing (ERF) compared to scenarios with no interannual variability in emissions. Satellite-estimated BB emissions (and associated variability) result in a June–September absolute ERF (relative to zero BB emissions) of -7.7 W m^{-2} from 50° to 70°N , compared to -10.4 W m^{-2} when no emissions variability is used in the Community Earth System Model version 2 (CESM2). This difference in forcing is attributable to nonlinear aerosol-cloud interactions. Aerosol forcing will be overestimated (i.e., more negative) if emissions are temporally-smoothed.

Plain Language Summary Aerosols are small particles in the air that can impact the climate, but we don't know exactly how much. One reason for this uncertainty is that the amount of aerosols can change a lot over time, especially when it comes from burning things like wood or plants (i.e., biomass burning emissions). When the amount of these biomass burning aerosols changes a lot from year-to-year, it has less of an impact on the climate. This is because clouds react less strongly when aerosol concentrations are high compared to when they are low. If we smooth out the changes in aerosol amounts over time (as is done with most Earth System Model simulations), we will overestimate their cooling impact on the climate.

1. Introduction

Atmospheric aerosols are a critical component of the climate system, but the complex processes governing their production, deposition, and interactions with clouds are difficult to observe and model. Uncertainty in the aerosol forcing is one of the greatest challenges for understanding historical climate change and projecting near-future climate evolution (Forster et al., 2021; Kiehl, 2007).

Previous research on aerosol radiative forcing has focused on the effect of secular change in aerosol emissions, with little consideration of the impact of shorter timescale variability in the emissions. For example, the fifth Coupled Model Intercomparison Project (CMIP5; Taylor et al., 2012) historical and future simulations use biomass burning (BB) emissions estimates that are smooth temporally compared to real-world emissions, particularly on inter- and sub-annual time scales. Real-world BB emissions in the extratropics occur episodically and stochastically, and may depend on weather conditions (precipitation, drought, lightning) or human activity (agricultural burning, forest clearing, arson) (Lamarque et al., 2010; van der Werf et al., 2017).

To incorporate more realistic aerosol emissions variability, the latest CMIP (sixth phase; CMIP6; Eyring et al., 2016) includes BB emissions estimates derived from satellite observations for historical simulations from 1997 to 2014 (Figure 1a; van Marle et al., 2017). Historical CMIP6 BB emissions in this time period have much higher temporal variability than those used in previous model intercomparison efforts (e.g., the CMIP5 historical simulations). However, the BB emissions used for CMIP6 prior to 1997 (before satellite measurement capability) are similar to the CMIP5 inventories, with weak temporal variability (Figure 1a black line; Lamarque et al., 2010; van Marle et al., 2017).

Recent analyses in the Community Earth System Model version 2 (CESM2; Danabasoglu et al., 2020) have estimated the climate effect of this change in BB emissions variability by comparing simulation scenarios

© 2023 The Authors.

This is an open access article under the terms of the [Creative Commons Attribution-NonCommercial License](https://creativecommons.org/licenses/by-nc/4.0/), which permits use, distribution and reproduction in any medium, provided the original work is properly cited and is not used for commercial purposes.

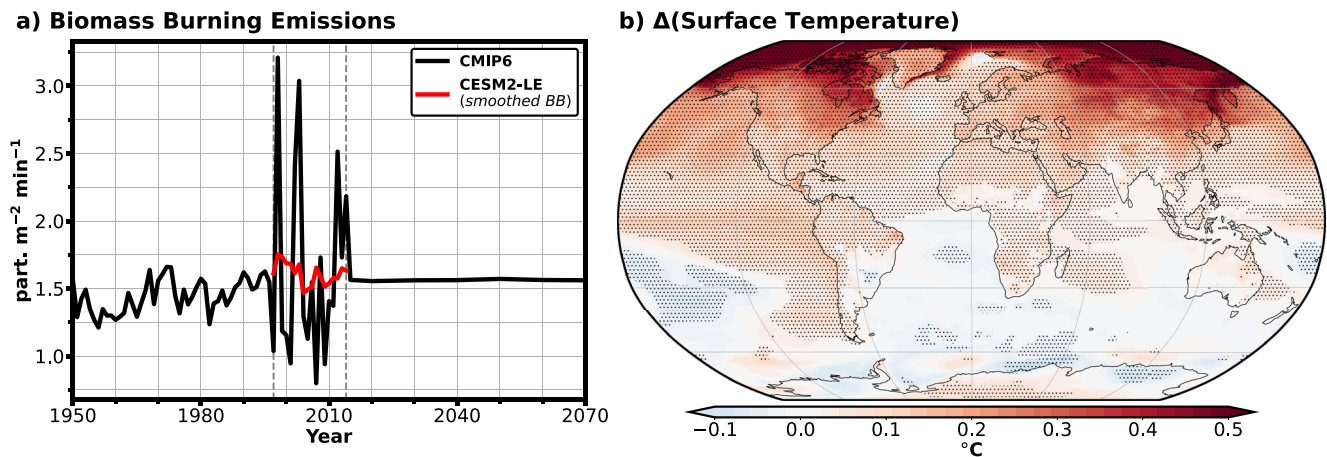


Figure 1. Biomass burning (BB) emissions used for CMIP6 and the effect of high BB emissions variability on surface temperature in CESM2. Panel (a) shows the annual mean biomass burning (BB) emissions averaged over 50°–70°N prescribed for CMIP6 (black line) and a second smoothed emissions inventory used for 50 members of the Community Earth System Model Large Ensemble version 2 (CESM2-LE) over the recent historical period (red line), in particles $\text{m}^{-2} \text{min}^{-1}$ (Text S2 in Supporting Information S1). The vertical gray dashed lines delineate the period of high BB emissions variability in the CMIP6 prescribed BB emissions (1997–2014). Panel (b) shows the difference in surface temperature between the CMIP6 emissions ensemble members and smoothed BB emissions ensemble members in the CESM2-LE during 1997–2014 (average of 50 CMIP6 emissions ensemble members minus average of 50 smoothed BB emissions ensemble members; in $^{\circ}\text{C}$). Stippling signifies 90% confidence (Text S8 in Supporting Information S1). See Text S1 in Supporting Information S1 for a further description of CESM2-LE and BB emissions therein.

with temporally-smoothed BB emissions to scenarios with time-varying CMIP6 emissions over the 1997 to 2014 period (DeRepenigny et al., 2022; Fasullo et al., 2022; Heyblom et al., 2022; Rodgers et al., 2021). The largest set of these comparison simulations is the CESM2 Large Ensemble (CESM2-LE; Figure 1a; Rodgers et al., 2021). Studies using the CESM2-LE show that the sudden change in BB emissions variability in the CMIP6 late-historical simulations leads to shifts in the climate, producing increases in simulated downwelling shortwave radiation and enhancing surface warming (Fasullo et al., 2022; also Figure 1b), increases in atmospheric water vapor and precipitation (Heyblom et al., 2022), and accelerated Arctic sea ice loss (DeRepenigny et al., 2022). These studies postulated that nonlinearities in the climate system's response to BB aerosols produced these climate effects. However, the coupled climate model simulations used in these studies did not allow for the decoupling of climate forcing and feedback, making attribution of the cause difficult.

Here, we use idealized Earth System Model (ESM) simulations to show that the temporal variability of BB aerosol emissions substantially impacts the magnitude of the forcing attributable to these emissions. We show that BB emissions variability impacts BB aerosol forcing because of a nonlinear response of aerosol-cloud interactions to atmospheric aerosol concentrations. Our study provides direct evidence that temporal variability of BB aerosol weakens the time-averaged aerosol cloud radiative effect in a state-of-the-art ESM, and that temporal smoothing will lead to a much stronger BB aerosol radiative effect.

2. Methods

To quantify the impact that greater interannual variability in biomass burning (BB) emissions has on the total radiative forcing attributable to these emissions, we conduct simulations using the Community Earth System Model version 2 (CESM2; Danabasoglu et al., 2020) with idealized BB emissions perturbations. In each simulation we configure CESM2 in the same way as the CESM2-LE (Text S1 in Supporting Information S1), but fix sea surface temperatures (SSTs), sea ice concentrations, and all forcings (except BB emissions) to the 2000 climatology (mean monthly values from 1995 to 2005). We use three different simulations, each of which treat BB emissions variability differently (Figure 2). Each simulation is run for 54 years.

The first simulation (hereafter “Real-Var”; Figure 2 green line) uses BB emissions as prescribed for CMIP6 historical simulations from 1997 to 2014 (van der Werf et al., 2017; van Marle et al., 2017). The emissions estimates for this period are thus taken to represent a best estimate of real-world BB emissions. These 18 years of emissions are repeated three times. The second simulation (hereafter “Pulse-Var”; Figure 2 yellow line) prescribes an idealized

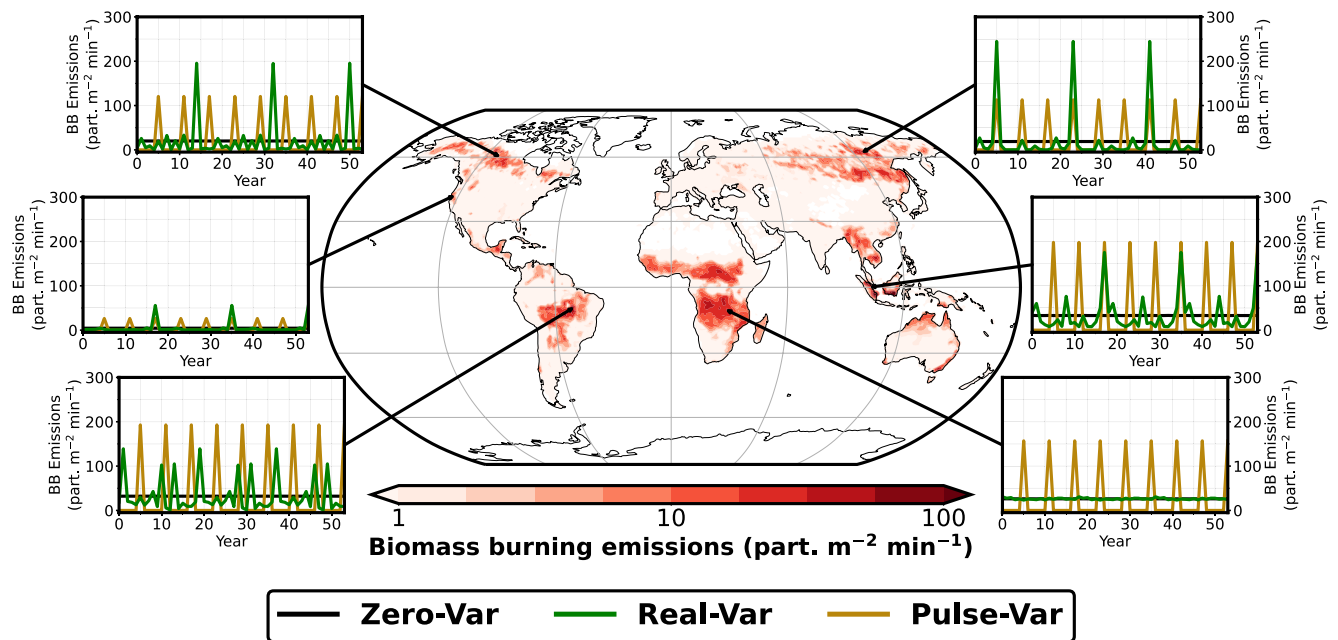


Figure 2. Idealized simulations to quantify changes in effective radiative forcing (ERF) due to biomass burning (BB) emissions variability. The center image shows the time-integrated emissions rate of BB emissions for all scenarios (in particles $\text{cm}^{-2} \text{s}^{-1}$; Text S2 in Supporting Information S1) in red, while the surrounding insets show the time evolution of BB emissions from Zero-Var, Real-Var, and Pulse-Var (black, green, and brown lines, respectively) at selected locations.

high-temporal variability emissions scenario where all emissions for each grid cell occur every 6 years in phase with all other grid cells. Total emissions in years that simulate a pulse of BB emissions are equal to six times the annual mean emissions from the Real-Var experiment at each grid cell; during other years BB emissions are zero. A third experiment (hereafter “Zero-Var”; Figure 2 black line) uses emissions based upon a climatology that repeats each year, and thus has no interannual variability in BB emissions. It is important to note that due to the aggregation of emissions in time, the Pulse- and Zero-Var inventories are also spatially smoother than the Real-Var inventory.

All simulations use fixed SSTs to allow the direct quantification of the effective radiative forcing (ERF) in the absence of most feedbacks (Text S3 in Supporting Information S1; Hansen et al., 2005; Forster et al., 2021). Because the time-integrated emissions are equal across these three simulations, differences in ERF are attributable entirely to differences in the variability of BB emissions.

In addition, we utilize the outcomes obtained from our fixed-SST simulations to create a heuristic model that illustrates the underlying mechanism responsible for the differences in ERF when variations in BB emissions variability are specified. To achieve this, we derive synthetic distributions that represent the aerosol concentrations present in the Zero-Var (black) and Real-Var (green) simulations by fitting normal and log-normal probability density functions to the Zero-Var and Real-Var simulation concentrations, respectively. We then demonstrate how each of these idealized aerosol concentration distributions leads to different distributions of cloud radiative effect (CRE).

3. Results

3.1. The Effects of Emissions Variability on the Aerosol Forcing

Figures 3a–3c shows that the BB aerosol effective radiative forcing (ERF) weakens (i.e., becomes less negative) when emissions vary in time (as in Real-Var and Pulse-Var) compared to when there is no interannual variability (as in Zero-Var). We denote the change in ERF due to BB emissions variability as $\Delta\text{ERF}_{\text{BBVar}}$, computed as the difference in the ERF between scenarios with time-varying emissions (Pulse-Var and Real-Var) and Zero-Var. The $\Delta\text{ERF}_{\text{BBVar}}$ is strongest over regions of high column-integrated aerosol concentration variability (Figure S1 in Supporting Information S1), particularly over the NH mid- to high-latitudes from June–September (JJAS; the

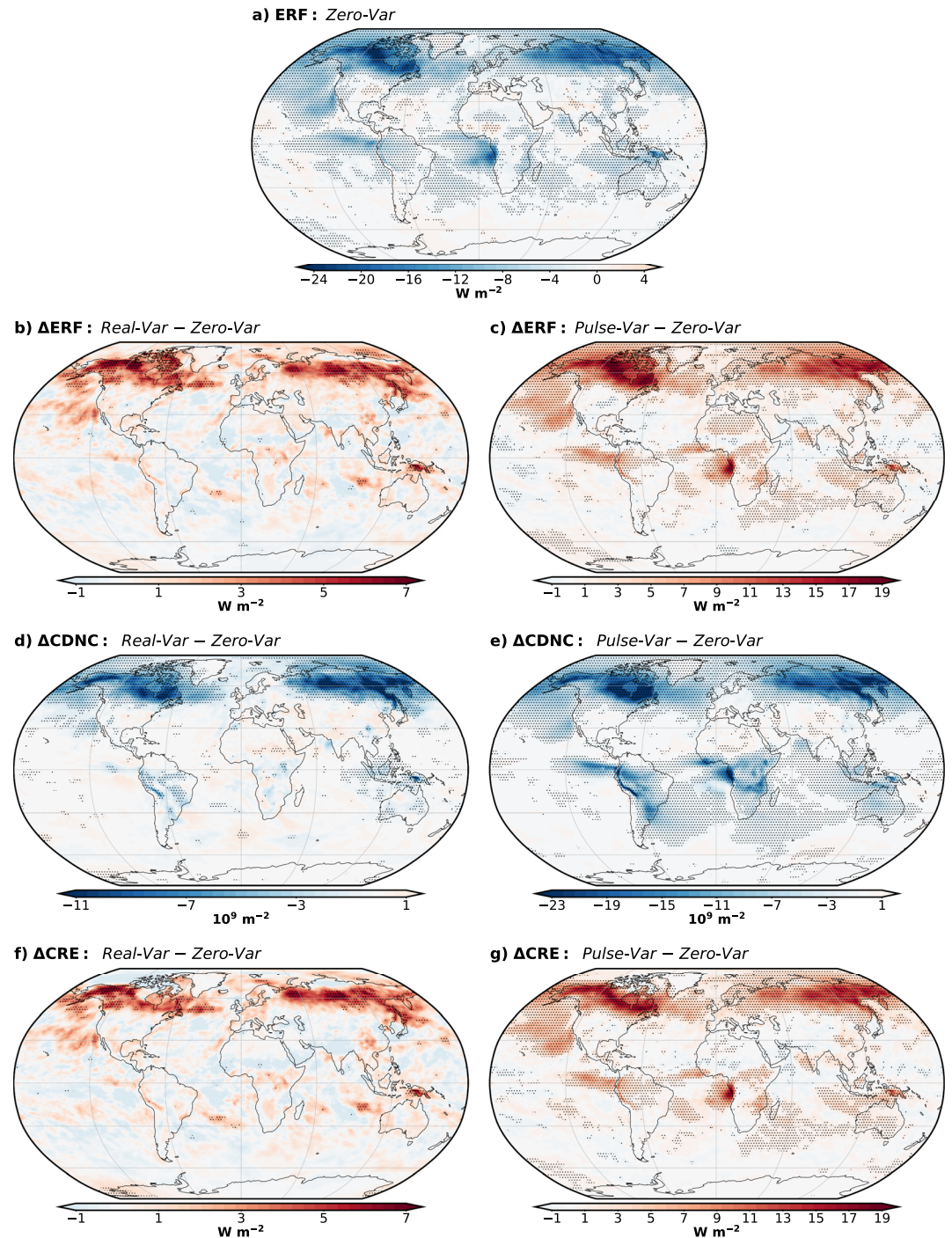


Figure 3. Change in effective radiative forcing (ERF) and cloud properties due to biomass burning emissions variability. Panel (a) shows the June–September (JJAS) mean absolute ERF due to BB emissions in the Zero-Var experiment (relative to no BB emissions). Panels (b)–(g) show the JJAS mean change in ERF (b and c; denoted Δ ERF_{BBVar}; in $W m^{-2}$), vertically integrated cloud droplet number concentration (d and e; CDNC; in $10^9 m^{-2}$), and total (long and shortwave) cloud radiative effect (f and g; CRE; in $W m^{-2}$) due to BB emissions variability in the Real-Var (left column) and Pulse-Var (right column) experiments. Changes due to BB emissions variability are defined as the variability experiments minus the Zero-Var experiment. Stippling signifies 90% confidence (Text S8 in Supporting Information S1).

period of most active fires in this region; see Figure S2 in Supporting Information S1 for annual mean difference). For example, averaged from 50° to 70°N, we find a +1.1 W m⁻² (+0.1 W m⁻² global) annual mean and +2.7 W m⁻² (+0.42 W m⁻² global) JJAS mean ERF weakening in the Real-Var experiment relative to Zero-Var. In effect, episodic BB emissions leads to a weaker (i.e., less negative) aerosol forcing associated with biomass burning.

3.2. Differences in Forcing Are Driven by Differences in the Cloud Radiative Effect

ERF sensitivity to emissions variability (i.e., $\Delta\text{ERF}_{\text{BBVar}}$) is due to a weaker time-averaged cloud response to aerosol emissions when BB emissions are variable. Figures 3d–3g shows how time-averaged cloud properties are affected by BB emissions variability. Each panel displays selected JJAS cloud property changes for the higher variability simulation compared to the Zero-Var simulation (Real-Var and Pulse-Var simulations in the left and right column respectively; also see Figure S3 in Supporting Information S1 for annual mean change). Averaged cloud droplet number concentration (CDNC; Figures 3d and 3e) is smaller in the simulations with higher interannual BB variability. Similar to ERF changes, the largest sensitivity in CDNC is found in regions where BB emissions interannual variability is large (i.e., predominately over the NH mid- to high-latitudes land regions). There are similar reductions in cloud amount and liquid water path with increased BB emissions variability (Figure S4 in Supporting Information S1).

The time-averaged increase in absorbed radiation due to changes in clouds is shown in Figures 3f and 3g as the cloud radiative effect (CRE). The CRE change due to BB emissions variability is highly correlated with $\Delta\text{ERF}_{\text{BBVar}}$: global Pearson pattern correlation coefficient of the annual means of 0.87 in the Real-Var experiment and 0.93 in the Pulse-Var experiment. These correlations, and the similar magnitudes of CRE and $\Delta\text{ERF}_{\text{BBVar}}$, indicate that $\Delta\text{ERF}_{\text{BBVar}}$ is driven by changes in time-averaged cloud properties when BB emissions are variable.

We note that there is a small region over Arctic land where there is increased absorbed radiation that is not due to changes in clouds (Figure S5a and S5b in Supporting Information S1; shown as clear-sky top of atmosphere net radiative flux). The increase in absorbed radiation in the absence of clouds is due to a decrease in land-surface albedo over the same region (Figure S5c and S5d in Supporting Information S1), which is a feedback resulting from the difference in forcing. Though the configuration and method used here to quantify the ERF is a widely accepted approach (Text S3 in Supporting Information S1; also see Hansen et al., 2005; Smith et al., 2020; Forster et al., 2021), it does allow for the possibility that computed changes in ERF are due differences in land-surface feedbacks not corrected for in our computation (Text S3 in Supporting Information S1). We replicated the Real-Var experiment in an aquaplanet configuration with CESM2 (in which land surfaces are replaced with an idealized ocean; Text S4 in Supporting Information S1; Marshall et al., 2007) and find qualitatively similar results (Figure S6 in Supporting Information S1). From this, we conclude the cloud response to BB emissions variability is not driven by land surface interactions. Though nonlinear land feedbacks, such as the land surface albedo, may be amplifying the change in ERF (as computed in this study) due to differences in BB emissions variability, they are not the driver of the model response.

3.3. Differences in Cloud Radiative Effect Are Due To Nonlinear Aerosol-Cloud Interactions

We now show that the time-averaged CRE weakens when BB emissions are more variable because of a nonlinear relationship between atmospheric aerosol concentrations and their effects on cloud properties. Nonlinearity in aerosol-cloud interactions are expected from both modeling and observational studies. As aerosol concentrations increase, they less effectively nucleate to become cloud droplets (Bougiatioti et al., 2016; Carslaw et al., 2013; Kacarab et al., 2020; Reutter et al., 2009; Rissman et al., 2004; Twomey, 1977). Because cloud droplet nucleation becomes less effective at higher aerosol concentrations, the relationship between aerosol concentration and CRE is nonlinear.

Figure 4 confirms that the time- and area-averaged relationship of CDNC and CRE is indeed nonlinear over 50°–70°N during JJAS. Shown in this figure are the cloud responses to varying fixed BB emissions rates (purple), as well as Real-Var (green) and Pulse-Var (yellow) simulations. Figure 4 also shows responses to varying aerosol concentrations in the CESM2-LE during the simulated high BB emissions variability period from 1997 to 2014 (blue; shown as probability density function). From the left column of Figure 4, it is clear that CDNC and CRE depend nonlinearly on aerosol concentration. This nonlinear response is apparent across the fixed aerosol emissions simulations, as well as in the Real-Var experiment and CESM2-LE.

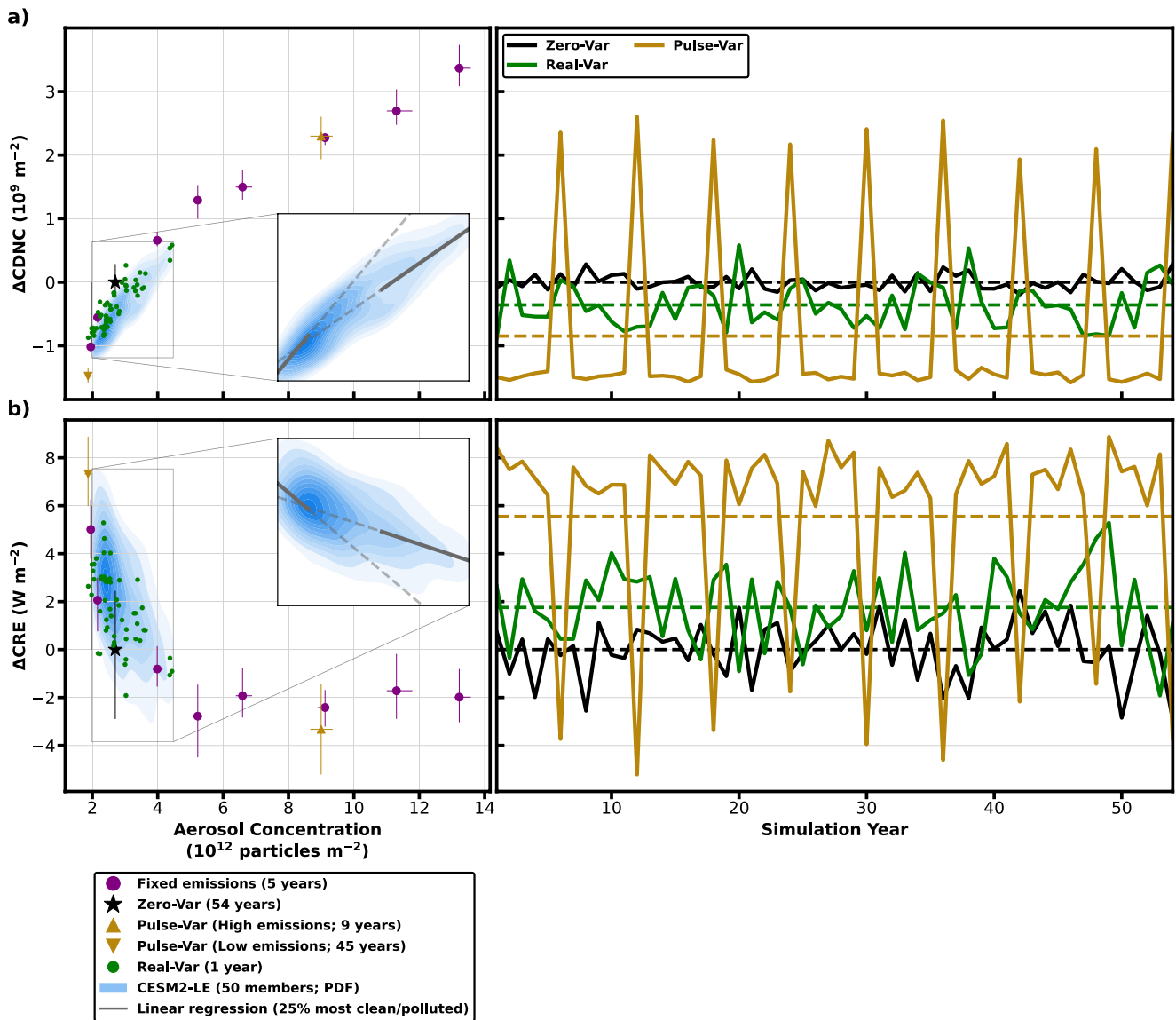


Figure 4. Responses of CDNC and CRE to varying aerosol emissions for June–September (JJAS) averaged over 50° – 70° N, relative to the Zero-Var simulations unless otherwise stated. The left column shows the relationship between column-integrated aerosol concentrations (in 10^{12} particles m^{-2} ; Text S2 in Supporting Information S1) and (a) column-integrated CDNC (in $10^9 m^{-2}$) or (b) CRE (in $W m^{-2}$) for a collection of years (number of years displayed in the legend) drawn from each experiment. The average and range of that collection is shown by marker and whiskers. The “High” and “Low” statistics are produced by averaging the years which do and do not have BB emissions in the Pulse-Var experiment, respectively. “Fixed emissions” experiments scale the Zero-Var BB emissions. CESM2-LE probability density functions (PDF) represent changes of each year in the high BB emissions variability simulations relative to the ensemble annual mean from the low BB emissions variability simulations of the CESM2-LE historical simulations from 1997 to 2014 (see Text S1 in Supporting Information S1 for a description of different CESM2-LE ensemble members). The right column shows the time evolution of CDNC and CRE from the Zero-Var, Real-Var, and Pulse-Var simulations. The horizontal dashed lines represent the JJAS mean for the entire simulation period.

The nonlinear response to BB emissions influences the temporal evolution of the simulations, seen in the right column of Figure 4. When emissions are higher than the Zero-Var case, the incremental change in CDNC and CRE is smaller in magnitude than when emissions are lower than the Zero-Var case. As a result, over low emissions years, there is a larger increase in absorbed solar energy (relative to the Zero-Var baseline) compared to the decrease in absorbed solar energy over high emissions years, explaining the time-averaged effects seen in Figure 3.

We use a heuristic model to further demonstrate how nonlinearities in aerosol-cloud interactions lead to a weakening of the time-averaged CRE if aerosol emissions are variable in time. Figure 5a shows distributions

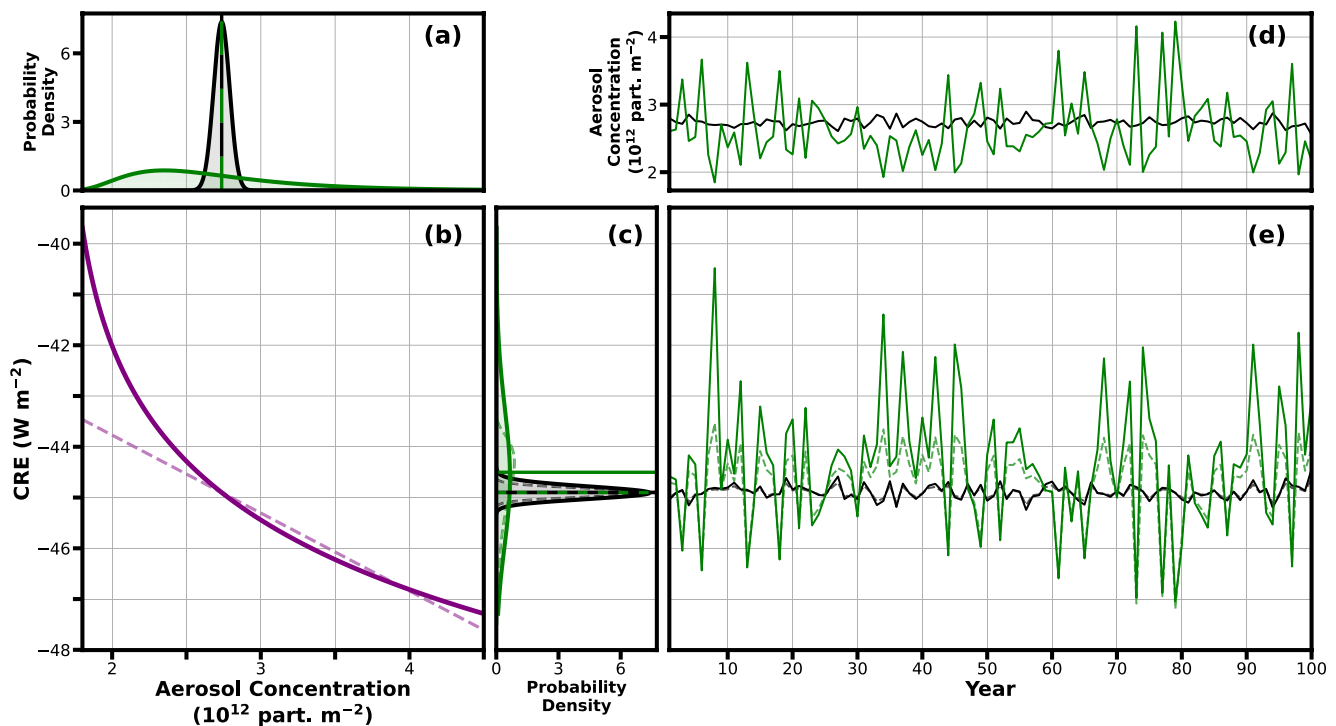


Figure 5. Idealized cloud radiative effect (CRE) response to varying aerosol concentrations. Panel (a) shows probability density functions (PDF) of aerosol concentrations representative of Real-Var and Zero-Var BB emissions scenarios (green and black, respectively). Panel (b) shows the cloud radiative effect (CRE) response to aerosol concentration derived from CESM2 (nonlinear; solid purple) and a linear response (dashed purple). Panel (c) shows the resulting CRE PDFs from the nonlinear and linear aerosol-CRE responses (solid and dashed lines, respectively). Vertical and horizontal lines in panels (a) and (c) represent the mean aerosol concentration and CRE, respectively, of each distribution. Panel (d) shows a 100-year aerosol concentration time series randomly drawn from the high and zero aerosol emissions variability PDFs (green and black lines, respectively). Panel (e) shows the resulting CRE from aerosol concentrations shown in panel (d) from the nonlinear and linear aerosol-CRE responses (solid and dashed lines, respectively).

representative of the 50° – 70° N area mean aerosol concentration resulting from emissions in the Zero-Var (normal distribution; black) and Real-Var (log-normal distribution; green) experiments, both of which have the same mean (overlapping vertical green and black lines). Note that the Zero-Var distribution has some variability (i.e., width) because of meteorological variability within these simulations, not BB emissions variability itself, which is nil. Figure 5b shows nonlinear (logarithmic; solid) and linear (dashed) functions describing two separate inferred relationships between aerosol concentrations and CRE, derived from Figure 4b (see Text S5 in Supporting Information S1 for further description).

Figure 5c shows the projected distributions of CRE using the functions shown in Figure 5b. Comparing CRE distributions resulting from nonlinear (solid lines) and linear (dashed lines) aerosol-CRE functions shows the effect of nonlinearity in the aerosol-CRE relationship (Figure 5c). First, any aerosol distribution will be skewed toward weakened CRE values as the nonlinear aerosol-CRE function deviates further from the linear function at lower aerosol concentrations than at higher concentrations. Second, realistic emissions variability (such as in Real-Var) has a much higher frequency of low concentration years (where the nonlinear relationship deviates the most from the linear function) compared to high concentration years, resulting in further CRE weakening. The combination of these two effects results in a weaker mean CRE for the log-normal aerosol concentration distribution when using the nonlinear aerosol-CRE function (horizontal solid green line) compared to the linear aerosol-CRE function (horizontal dashed green and black lines). We note that the mean CRE is also weaker for the normal aerosol concentration distribution when using the nonlinear aerosol-CRE function (horizontal solid black line) compared to if the linear aerosol-CRE function is used, though the change is small (and not visible on Figure 5c) as the variability is low.

Two synthetic time series of aerosol concentrations (Figure 5d) and the resulting CRE values (Figure 5e) confirm the time-averaged effect leading to differences in mean CRE shown in the time series in Figure 4. When emissions are low (and CRE is less negative), a nonlinear aerosol-CRE relationship results in much weaker (less

negative) CRE values than if the relationship is linear (compare large positive deviations in CRE due to nonlinear and linear aerosol-CRE relationships).

4. Discussion

4.1. A Need for More Idealized Experiments

To-date, there have been few sets of experiments that can be used to infer the impacts of BB emissions variability on the climate system. To the best of our knowledge, there has only been experiments conducted by Fasullo et al. (2022) and DeRepentigny et al. (2022), the CESM2-LE (Rodgers et al., 2021), and those performed for this study (Methods). As the only difference in forcing is the treatment of BB emissions variability, these experiments can be used to directly quantify the impact of BB emissions variability on the climate. Furthermore, we have conducted a set of idealized ESM simulations that allow us to quantify the difference in radiative forcing attributed to BB emissions variability.

It is important to assess how the radiative forcing is affected in more ESMs to understand how model-specific aerosol and cloud microphysics parameterizations may affect the forcing uncertainty attributable to aerosol emissions variability. For example, $\Delta\text{ERF}_{\text{BBVar}}$ may be particularly noticeable in CESM2 as it has relatively strong aerosol-cloud interactions (Smith et al., 2020). Understanding the strength of the $\Delta\text{ERF}_{\text{BBVar}}$ in ESMs is important for the design of future intercomparisons. Further idealized experiments, such as those described here, are necessary to detect and quantify the effect of aerosol variability on the effective radiative forcing due to aerosol-cloud interactions in a variety of ESMs. Current model intercomparison projects (i.e., those for CMIP6) are not adequate to attribute changes in the climate to differences in BB emissions variability because it is unlikely that quantifying statistically robust differences in climate is feasible without a direct comparison between high and low BB emissions variability scenarios. Indeed, we find no robust evidence of nonlinearity between annual BB emissions and CRE in individual ESM output submitted to the CMIP6 historical Atmospheric Model Intercomparison Project (AMIP; Figure S7 in Supporting Information S1; Text S7 in Supporting Information S1; Gates et al., 1999; Eyring et al., 2016).

4.2. Implications

The temporal variability in BB aerosol emissions changes the climate forcing attributable to these aerosols. In particular, we show that realistic BB emissions variability leads to a weaker (less negative) forcing, compared to low emissions variability. This effect is particularly strong and widespread over the NH mid- to high-latitudes. This ERF change (reduction in the magnitude of the total aerosol forcing) induced by BB emissions variability is due to nonlinear aerosol-cloud interaction effects.

These findings are of particular importance when considering the total aerosol forcing over historical periods and into the future. Most emissions inventories neglect realistic interannual variability (e.g., Hoesly et al., 2018; O'Neill et al., 2016; van Marle et al., 2017), which would lead to a more negative ERF due to aerosol-cloud interaction effects (ERF_{ACI}). Furthermore, many modeling approaches used to evaluate ERF_{ACI} do not prescribe realistic variability in aerosol emissions, if at all. For example, the Radiative Forcing Model Intercomparison Project (RFMIP) uses either fixed present-day or CMIP6 historical aerosol emissions that include only secular trends to quantify the radiative forcing of aerosols in CMIP6 ESMs; they do not include realistic BB emissions variability prior to 1997 (Pincus et al., 2016). Likewise, emissions prescribed for future projection scenarios (after 2014) also neglect temporal variability in aerosol emissions (recall Figure 1a; Riahi et al., 2017). We also note that, while the issues have been discussed here in the context of the interannual variability of BB emissions, these issues are likely relevant to other emissions sources that are sensitive to natural and anthropogenic variability (e.g., DMS emissions that are sensitive to ocean variability).

As treatments of aerosol variability differ in the historical, present-day, and future scenario simulations, significant biases in the total aerosol forcing may be present. The inclusion of interannual variability for some years, and neglect of it in others, will introduce discrepancies and discontinuities in the aerosol forcing that may be significant (such as spurious sea ice trends, as shown in DeRepentigny et al., 2022). To properly evaluate aerosol forcings and model past, present, and future climates, the temporal variability of aerosol emissions should be treated consistently and more realistically.

Past (prior to the satellite era) and future biomass burning aerosol emissions (and thus their variability) are uncertain. They will depend on many different factors, including changes in fire weather and fuel loads. As ESMs simulate aerosol-cloud interactions using more and more complex physics, they must also consider how BB aerosol emissions variability has changed through the past and into the future. Ideally, emissions variability should be prescribed with a carefully stated, well understood set of assumptions with impacts that can be evaluated and quantified. Alternatively, to avoid any assumptions of emissions variability, prognostic fire models should be integrated into the next generation of ESMs.

Data Availability Statement

This material is based upon work supported by the National Center for Atmospheric Research (NCAR). CESM2-LE data are available here <https://www.cesm.ucar.edu/community-projects/lens2>. Information on the release of the CESM2-LE is available here <https://doi.org/10.5194/esd-12-1393-2021>. The CMIP6 data used for calculating cloud radiative effects from multiple Earth System Models (see Figure S7 in Supporting Information S1) are publicly available through the World Climate Research Programme CMIP6 website (<https://esgf-node.llnl.gov/search/cmip6/>).

References

- Bougiatioti, A., Bezantakos, S., Stavroulas, I., Kalivitis, N., Kokkalis, P., Biskos, G., et al. (2016). Biomass-burning impact on CCN number, hygroscopicity and cloud formation during summertime in the eastern Mediterranean. *Atmospheric Chemistry and Physics*, 16(11), 7389–7409. <https://doi.org/10.5194/acp-16-7389-2016>
- Carlsaw, K. S., Lee, L. A., Reddington, C. L., Pringle, K. J., Rap, A., Forster, P. M., et al. (2013). Large contribution of natural aerosols to uncertainty in indirect forcing. *Nature*, 503(7474), 67–71. <https://doi.org/10.1038/nature12674>
- Danabasoglu, G., Lamarque, J.-F., Bacmeister, J., Bailey, D. A., DuVivier, A. K., Edwards, J., et al. (2020). The Community Earth System Model Version 2 (CESM2). *Journal of Advances in Modeling Earth Systems*, 12(2), e2019MS001916. <https://doi.org/10.1029/2019MS001916>
- DeRepentigny, P., Jahn, A., Holland, M. M., Kay, J. E., Fasullo, J., Lamarque, J.-F., et al. (2022). Enhanced simulated early 21st century Arctic sea ice loss due to CMIP6 biomass burning emissions. *Science Advances*, 8(30), eabo2405. <https://doi.org/10.1126/sciadv.abo2405>
- Eyring, V., Bony, S., Meehl, G. A., Senior, C. A., Stevens, B., Stouffer, R. J., & Taylor, K. E. (2016). Overview of the Coupled Model Intercomparison Project Phase 6 (CMIP6) experimental design and organization. *Geoscientific Model Development*, 9(5), 1937–1958. <https://doi.org/10.5194/gmd-9-1937-2016>
- Fasullo, J. T., Lamarque, J.-F., Hannay, C., Rosenbloom, N., Tilmes, S., DeRepentigny, P., et al. (2022). Spurious late historical-era warming in CESM2 driven by prescribed biomass burning emissions. *Geophysical Research Letters*, 49(2), e2021GL097420. <https://doi.org/10.1029/2021GL097420>
- Forster, P., Storelvmo, T., Armour, K., Collins, W., Dufresne, J.-L., Frame, D., et al. (Eds.). (2021). *Climate change 2021: The physical science basis. Contribution of working group I to the sixth assessment report of the intergovernmental panel on climate change* (pp. 923–1054). Cambridge University Press. <https://doi.org/10.1017/9781009157896.009>
- Gates, W. L., Boyle, J. S., Covey, C., Dease, C. G., Doutriaux, C. M., Drach, R. S., et al. (1999). An overview of the results of the atmospheric model intercomparison project (AMIP I). *Bulletin of the American Meteorological Society*, 80(1), 29–55. [https://doi.org/10.1175/1520-0477\(1999\)080<0029:A00TRO>2.0.CO;2](https://doi.org/10.1175/1520-0477(1999)080<0029:A00TRO>2.0.CO;2)
- Hansen, J., Sato, M., Ruedy, R., Nazarenko, L., Lacis, A., Schmidt, G. A., & Zhang, S. (2005). Efficacy of climate forcings. *Journal of Geophysical Research*, 110(D18), D18104. <https://doi.org/10.1029/2005JD005776>
- Heyblom, K. B., Singh, H. A., Rasch, P. J., & DeRepentigny, P. (2022). Increased variability of biomass burning emissions in CMIP6 amplifies hydrologic cycle in the CESM2 large ensemble. *Geophysical Research Letters*, 49(5), e2021GL096868. <https://doi.org/10.1029/2021GL096868>
- Hoesly, R. M., Smith, S. J., Feng, L., Klimont, Z., Janssens-Maenhout, G., Pitkanen, T., et al. (2018). Historical (1750–2014) anthropogenic emissions of reactive gases and aerosols from the Community Emissions Data System (CEDS). *Geoscientific Model Development*, 11(1), 369–408. <https://doi.org/10.5194/gmd-11-369-2018>
- Kacarab, M., Thornhill, K. L., Dobracki, A., Howell, S. G., O'Brien, J. R., Freitag, S., et al. (2020). Biomass burning aerosol as a modulator of the droplet number in the southeast Atlantic region. *Atmospheric Chemistry and Physics*, 20(5), 3029–3040. <https://doi.org/10.5194/acp-20-3029-2020>
- Kiehl, J. T. (2007). Twentieth century climate model response and climate sensitivity. *Geophysical Research Letters*, 34(22), L22710. <https://doi.org/10.1029/2007GL031383>
- Lamarque, J.-F., Bond, T. C., Eyring, V., Granier, C., Heil, A., Klimont, Z., et al. (2010). Historical (1850–2000) gridded anthropogenic and biomass burning emissions of reactive gases and aerosols: Methodology and application. *Atmospheric Chemistry and Physics*, 10(15), 7017–7039. <https://doi.org/10.5194/acp-10-7017-2010>
- Marshall, J., Ferreira, D., Campin, J.-M., & Enderton, D. (2007). Mean climate and variability of the atmosphere and ocean on an aquaplanet. *Journal of the Atmospheric Sciences*, 64(12), 4270–4286. <https://doi.org/10.1175/2007JAS2226.1>
- O'Neill, B. C., Tebaldi, C., van Vuuren, D. P., Eyring, V., Friedlingstein, P., Hurtt, G., et al. (2016). The Scenario Model Intercomparison Project (ScenarioMIP) for CMIP6. *Geoscientific Model Development*, 9(9), 3461–3482. <https://doi.org/10.5194/gmd-9-3461-2016>
- Pincus, R., Forster, P. M., & Stevens, B. (2016). The Radiative Forcing Model Intercomparison Project (RFMIP): Experimental protocol for CMIP6. *Geoscientific Model Development*, 9(9), 3447–3460. <https://doi.org/10.5194/gmd-9-3447-2016>
- Reutter, P., Su, H., Trentmann, J., Simmel, M., Rose, D., Gunthe, S. S., et al. (2009). Aerosol- and updraft-limited regimes of cloud droplet formation: Influence of particle number, size and hygroscopicity on the activation of cloud condensation nuclei (CCN). *Atmospheric Chemistry and Physics*, 14(18), 7067–7080. <https://doi.org/10.5194/acp-9-7067-2009>
- Riahi, K., van Vuuren, D. P., Kriegler, E., Edmonds, J., O'Neill, B. C., Fujimori, S., et al. (2017). The shared socioeconomic pathways and their energy, land use, and greenhouse gas emissions implications: An overview. *Global Environmental Change*, 42, 153–168. <https://doi.org/10.1016/j.gloenvcha.2016.05.009>

Acknowledgments

K.B.H. is supported by the Natural Sciences and Engineering Council of Canada (NSERC) and the University of Victoria. H.A.S. is supported by base research support through the University of Victoria. H.H. is supported by DARPA-AIE-ACTM-AIBEDO. Computing resources, including the Cheyenne (<https://doi.org/10.5065/D6RX99HX>) high-performance computing system, were provided by the Computational and Information Systems Laboratory (CISL) at the National Center for Atmospheric Research (NCAR). All authors would like to acknowledge the CESM2 Large Ensemble Community Project and super-computing resources provided by the IBS Center for Climate Physics in South Korea. The CESM project is supported by NCAR, which is a major facility sponsored by the NSF under Cooperative Agreement No. 1852977.

- Rissman, T. A., Nenes, A., & Seinfeld, J. H. (2004). Chemical amplification (or dampening) of the Twomey effect: Conditions derived from droplet activation theory. *Journal of the Atmospheric Sciences*, *61*(8), 919–930. [https://doi.org/10.1175/1520-0469\(2004\)061<0919:CAODOT>2.0.CO;2](https://doi.org/10.1175/1520-0469(2004)061<0919:CAODOT>2.0.CO;2)
- Rodgers, K. B., Lee, S.-S., Rosenbloom, N., Timmermann, A., Danabasoglu, G., Deser, C., et al. (2021). Ubiquity of human-induced changes in climate variability. *Earth System Dynamics*, *12*(4), 1393–1411. <https://doi.org/10.5194/esd-12-1393-2021>
- Smith, C. J., Kramer, R. J., Myhre, G., Alterskjær, K., Collins, W., Sima, A., et al. (2020). Effective radiative forcing and adjustments in CMIP6 models. *Atmospheric Chemistry and Physics*, *20*(16), 9591–9618. <https://doi.org/10.5194/acp-20-9591-2020>
- Taylor, K. E., Stouffer, R. J., & Meehl, G. A. (2012). An overview of CMIP5 and the experiment design. *Bulletin of the American Meteorological Society*, *93*(4), 485–498. <https://doi.org/10.1175/BAMS-D-11-00094.1>
- Twomey, S. (1977). The influence of pollution on the shortwave albedo of clouds. *Journal of the Atmospheric Sciences*, *34*(7), 1149–1152. [https://doi.org/10.1175/1520-0469\(1977\)034<1149:TROPOT>2.0.CO;2](https://doi.org/10.1175/1520-0469(1977)034<1149:TROPOT>2.0.CO;2)
- van der Werf, G. R., Randerson, J. T., Giglio, L., van Leeuwen, T. T., Chen, Y., Rogers, B. M., et al. (2017). Global fire emissions estimates during 1997–2016. *Earth System Science Data*, *9*(2), 697–720. <https://doi.org/10.5194/essd-9-697-2017>
- van Marle, M. J. E., Kloster, S., Magi, B. I., Marlon, J. R., Daniou, A.-L., Field, R. D., et al. (2017). Historic global biomass burning emissions for CMIP6 (BB4CMIP) based on merging satellite observations with proxies and fire models (1750–2015). *Geoscientific Model Development*, *10*(9), 3329–3357. <https://doi.org/10.5194/gmd-10-3329-2017>